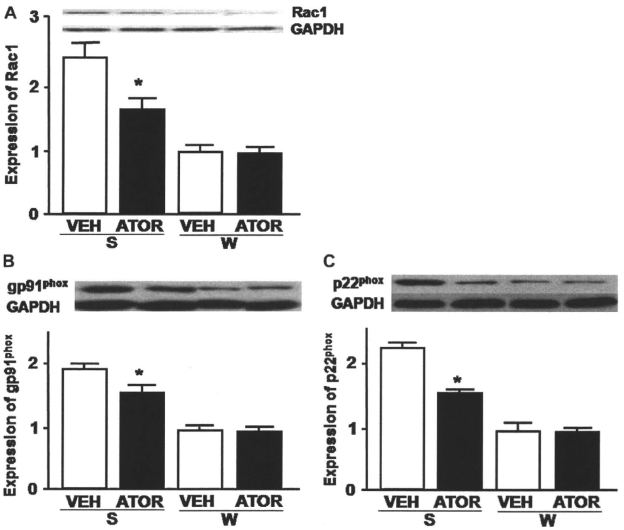

FIGURE 4. Western blot analysis showing the level of expression of Rac1 (A), gp91^{phox} (B), and p22^{phox} (C) in the membrane fraction of the RVLM at day 14 in ATOR- or VEH-treated SHRSP or WKY (n = 5 for each). *$P < 0.05$ for ATOR versus VEH in each strain. †$P < 0.05$ compared with VEH-treated WKY. The expression level of Rac1, gp91^{phox}, and p22^{phox} was expressed relative to that in W-VEH, which was assigned a value of 1. Data are shown as mean ± standard error of the mean.

In the present study, we measured SNA by spectral analysis. Low frequency power of SBP was computed by integrating the spectra between 0.04 and 0.15 Hz, and SNA is presented as LFnuSBP, as described in previous reports.[29–31] On day 14, the LFnuSBP values were comparable to those of uNE. Therefore, this method seems to be useful for measuring SNA in awake animals. Furthermore, atorvastatin improved the impaired baroreflex control in the SHRSP in the present study. Whereas we did not measure cardiac output in the present study and the reduction of BP and HR due to atorvastatin might cause a potential fall in cardiac output, the effects of atorvastatin are due to the decrease in sympathetic nerve activity. It is generally accepted that SNA is enhanced in SHRSP,[3,5,26–28,40] and atorvastatin attenuates the enhanced central sympathetic outflow to various organs including heart, kidney, and vasculature. At least, atorvastatin did not induce heart failure due to low cardiac output. We consider that the decrease in central sympathetic outflow reduced the peripheral vascular resistance by which cardiac output keep constant instead of the reduction of sympathetic outflow to the heart.

Another intriguing finding of the present study is that the BP-lowering and sympathoinhibitory effects are comparable between oral administration (50 mg/kg^{-1}/day^{-1})[7] and ICV injection (2 μg/kg^{-1}/day^{-1}) of atorvastatin. We confirmed the direct effects of atorvastatin administered into the brain on BP, SNA, and baroreflex function in SHRSP as one of the hypertensive models in the present study. The changes in TBARS levels are also similar between oral administration and ICV injection of atorvastatin. In SHRSP, the blood–brain barrier might be disrupted[38] and oral administration of atorvastatin is considered to affect the brain directly.[39] The present findings suggest that orally administered atorvastatin crosses the blood–brain barrier and affects the brain of SHRSP. The abnormal activation of sympathetic nervous system causes hypertension, heart failure, and ischemic heart diseases, and we consider that oral administration of atorvastatin has a potential to treat cardiovascular diseases due to the sympathoinhibition through the antioxidant effect in the RVLM.

We previously demonstrated that oral administration of atorvastatin increases the expression of endothelial nitric oxide synthase (eNOS) in the brainstem.[40] Overexpression of eNOS in the RVLM decreases SNA in WKY and SHRSP.[26–28] In the present study, we did not investigate whether an increase in NO production in the RVLM is involved in the reduction of BP and oxidative stress. It is possible, however, that ICV injection of atorvastatin increases eNOS in the RVLM of SHRSP and that an increase in eNOS contributes to the sympathoinhibitory effect. Further study is needed to clarify this issue.

In WKY rats, atorvastatin does not alter SNA and oxidative stress in the RVLM; these results are compatible with our previous report.[7] Moreover, atorvastatin also does not alter Rac1-induced NAD(P)H oxidase activity and Mn-SOD activity in the RVLM of WKY rats. In the present study, the mechanisms by which atorvastatin affected Rac1-induced NAD(P)H oxidase activity and Mn-SOD activity in SHRSP, but not in WKY, were not determined. It may be that there are thresholds for the induction of Rac1-induced NAD(P)H oxidase activity and Mn-SOD activity in the RVLM, which

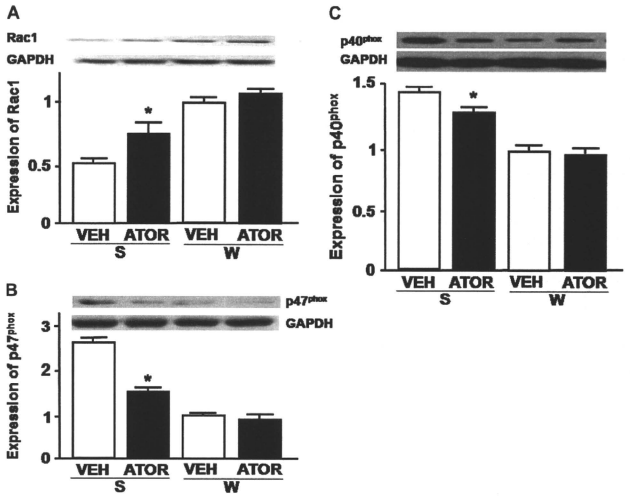

FIGURE 5. Western blot analysis showing the level of expression of Rac1 (A), $p47^{phox}$ (B), and $p40^{phox}$ (C) in the cytosolic fraction of the RVLM at day 14 in ATOR- or VEH-treated SHRSP or WKY (n = 5 per group). $*P < 0.05$ for ATOR versus VEH in each strain. $\dagger P < 0.05$ compared with VEH-treated WKY. The expression level of Rac1, $p47^{phox}$, and $p40^{phox}$ was expressed relative to that in W-VEH, which was assigned a value of 1. Data are shown as mean ± standard error of the mean.

are differently affected by atorvastatin between SHRSP and WKY rats.

STUDY LIMITATIONS

The present study has several limitations. First, we examined the effects of atorvastatin specifically in only the RVLM, and its effects in other brain areas cannot be excluded at this time. Nevertheless, neural activity in the RVLM has a direct influence on SNA,[1,2] and the present results identified an antioxidant effect of atorvastatin and its mechanisms in the RVLM. Angiotensin II type 1 receptors (AT_1R) are abundantly distributed in the RVLM, and there is a close link between AT_1R stimulation and NAD(P)H oxidase activation.[41] Therefore, in the present study, we focused on the RVLM, although other brain regions related to central autonomic control also contain AT_1R and NAD(P)H oxidase. Second, among all statins, we only studied the effect of atorvastatin, which is a lipophilic statin.[42] Our previous studies suggested that oral atorvastatin also reduces oxidative stress in the RVLM.[7] Further study is needed to clarify whether our results in the present study are broad class effects or are specific for atorvastatin. Finally, a recent study suggests that statins reduce BP in patients with hypertension.[43] It will be important to determine whether atorvastatin has this beneficial effect caused by the mechanism related to our suggestion in the present study, although we understand that this is difficult to examine in humans.

CONCLUSIONS

In conclusion, atorvastatin administered directly into the brain of SHRSP decreases BP, SNA, and baroreflex function. The findings of the present study suggest that these effects are associated with inhibition of oxidative stress in the RVLM, probably resulting from a decrease in NAD(P)H oxidase activity and the upregulation of Mn-SOD activity in the RVLM.

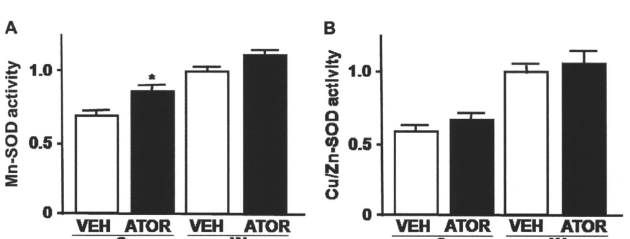

FIGURE 6. The activities of Mn-SOD (A) and Cu/Zn-SOD (B) in the RVLM at day 14 in ATOR- or VEH-treated SHRSP or WKY (n = 5 for each). $*P < 0.05$ for ATOR versus VEH in each strain. $\dagger P < 0.05$ compared with VEH-treated WKY. The activities of Mn-SOD and Cu/Zn-SOD were expressed relative to that in W-VEH, which was assigned a value of 1. Data are shown as mean ± standard error of the mean.

ACKNOWLEDGMENTS

We are grateful to Pfizer, Inc for supplying atorvastatin.

REFERENCES

1. Dampney RAL. Functional organization of central pathways regulating the cardiovascular system. *Physiol Rev.* 1994;74:323–364.
2. Guyenet PG. The sympathetic control of blood pressure. *Nat Rev Neurosci.* 2006;7:335–346.
3. Kishi T, Hirooka Y, Kimura Y, et al. Increased reactive oxygen species in rostral ventrolateral medulla contribute to neural mechanisms of hypertension in stroke-prone spontaneously hypertensive rats. *Circulation.* 2004;109:2357–2362.
4. Peterson JR, Sharma RV, Davisson RL. Reactive oxygen species in the neuropathogenesis of hypertension. *Curr Hypertens Rep.* 2006;8:232–241.
5. Hirooka Y. Role of reactive oxygen species in brainstem in neural mechanisms of hypertension. *Auton Neurosci.* 2008;142:20–24.
6. Sheh YL, Hsu C, Chan SHH, et al. NADPH oxidase- and mitochondrion-derived superoxide at rostral ventrolateral medulla in endotoxin-induced cardiovascular depression. *Free Radic Biol Med.* 2007;42:1610–1623.
7. Kishi T, Hirooka Y, Shimokawa H, et al. Atorvastatin reduces oxidative stress in the rostral ventrolateral medulla of stroke-prone spontaneously hypertensive rats. *Clin Exp Hypertens.* 2008;30:3–11.
8. Pliquett RU, Cornish KG, Peuler JD, et al. Simvastatin normalizes autonomic neural control in experimental heart failure. *Circulation.* 2003; 107:2493–2498.
9. Gao L, Wang W, Li YL, et al. Simvastatin therapy normalizes sympathetic neural control in experimental heart failure: roles of angiotensin II type 1 receptors and NAD(P)H oxidase. *Circulation.* 2005;112:1763–1770.
10. Gao L, Wang W, Zucker IH. Simvastatin inhibits central sympathetic outflow in heart failure by a nitric-oxide synthase mechanism. *J Pharmacol Exp Ther.* 2008;326:278–285.
11. Zimmerman MC, Dunlay RP, Lazartigues E, et al. Requirement for Rac1-dependent NADPH oxidase in the cardiovascular and dipsogenic actions of angiotensin II in the brain. *Circ Res.* 2004;95:532–539.
12. Nozoe M, Hirooka Y, Koga Y, et al. Inhibition of Rac1-derived reactive oxygen species in NTS decreases blood pressure and heart rate in stroke-prone SHR. *Hypertension.* 2007;50:62–68.
13. Byrne JA, Grieve DJ, Bendall JK, et al. Contrasting roles of NADPH oxidase isoforms in pressure-overload versus angiotensin II-induced cardiac hypertrophy. *Circ Res.* 2003;93:802–805.
14. Privratsky JR, Wold LE, Sowers JR, et al. AT1 blockade prevents glucose-induced cardiac dysfunction in ventricular myocytes: role of the AT1 receptor and NADPH oxidase. *Hypertension.* 2003;42:206–212.
15. Maach C, Kartes T, Killer H. Oxygen free radical release in human failing myocardium is associated with increased activity of Rac1-GTPase and represents a target for statin treatment. *Circulation.* 2003;108:1567–1574.
16. Wassmann S, Laufs U, Muller K, et al. Cellular antioxidant effects of atorvastatin in vitro and in vivo. *Arterioscler Thromb Vasc Biol.* 2002;22: 300–305.
17. Riad A, Du J, Stiehl S, et al. Low-dose treatment with atorvastatin leads to anti-oxidative and anti-inflammatory effects in diabetes mellitus. *Eur J Pharmacol.* 2007;569:204–211.
18. Habibi J, Whaley-Connell A, Qazi MA, et al. Rosuvastatin, a 3-hydroxy-3-methylglutaryl coenzyme A reductase inhibitor, decreases cardiac oxidative stress and remodeling in Ren2 transgenic rats. *Endocrinology.* 2007;148:2181–2188.
19. Whaley-Connell A, Habibi J, Nistala R, et al. Attenuation of NADPH oxidase activation and glomerular filtration barrier remodeling with statin treatment. *Hypertension.* 2008;51:474–480.
20. Chen X, Touyz RM, Park JB, et al. Antioxidant effects of vitamin C and E are associated with altered activation of vascular NADPH oxidase and superoxide dismutase in stroke-prone SHR. *Hypertension.* 2001;38: 606–611.
21. Carneado J, Alvarez de Sotomayor M, Perez-Guerrero C, et al. Simvastatin improves endothelial function in spontaneously hypertensive rats through a superoxide dismutase mediated antioxidant effect. *J Hypertens.* 2002;20:429–437.
22. Yilmaz MI, Baykal Y, Kilic M, et al. Effects of statins on oxidative stress. *Biol Trace Elem Res.* 2004;98:119–127.
23. Umeji K, Umemoto S, Itoh S, et al. Comparative effects of pitavastatin and probucol on oxidative stress, Cu/Zn superoxide dismutase, PPAR-gamma, and aortic stiffness in hypercholesterolemia. *Am J Physiol.* 2006;291: H2522–H2532.
24. Nozoe M, Hirooka Y, Koga Y, et al. Mitochondria-derived reactive oxygen species mediate sympathoexcitation induced by angiotensin II in the rostral ventrolateral medulla. *J Hypertens.* 2008;26:2176–2184.
25. Nishimura M, Takahashi H, Yoshimura M. Upregulation of the brain renin-angiotensin system in rats with chronic renal failure. *Acta Physiol (Oxf).* 2007;189:369–377.
26. Kishi T, Hirooka Y, Sakai K, et al. Overexpression of eNOS in the RVLM causes hypotension and bradycardia via GABA release. *Hypertension.* 2001;38:896–901.
27. Kishi T, Hirooka Y, Ito K, et al. Cardiovascular effects of overexpression of endothelial nitric oxide synthase in the rostral ventrolateral medulla in stroke-prone spontaneously hypertensive rats. *Hypertension.* 2002;39: 264–268.
28. Kishi T, Hirooka Y, Kimura Y, et al. Overexpression of eNOS in RVLM improves impaired baroreflex control of heart rate in SHRSP. *Hypertension.* 2003;41:255–260.
29. Castiglioni P, Di Rienzo M, Veicsteinas A, et al. Mechanisms of blood pressure and heart rate variability: an insight from low-level paraplegia. *Am J Physiol.* 2007;292:R1502–R1509.
30. Cerutti C, Gustin MP, Paultre CZ. Autonomic nervous system and cardiovascular variability in rats: a spectral analysis approach. *Am J Physiol.* 1991;261:H1292–H1299.
31. Pagani M, Montano N, Porta A, et al. Relationship between spectral components of cardiovascular variabilities, and direct measures of muscle sympathetic nerve activity in humans. *Circulation.* 1997;95:1441–1448.
32. Waki H, Kasparov S, Wong LF, et al. Chronic inhibition of eNOS activity in nucleus tractus solitarii enhances baroreceptor reflex in conscious rats. *J Physiol.* 2003;546:233–242.
33. Waki H, Katahira K, Polson JW, et al. Automation of analysis of cardiovascular autonomic function from chronic measurements of arterial pressure in conscious rats. *Exp Physiol.* 2006;91:201–213.
34. Braga VA, Burmeister MA, Sharma RV, et al. Cardiovascular responses to peripheral chemoreflex activation and comparison of different methods to evaluate baroreflex gain in conscious mice using telemetry. *Am J Physiol.* 2008;295:R1168–R1174.
35. Tai MH, Wang LL, Wu KL, et al. Increased superoxide anion in rostral ventrolateral medulla contributes to hypertension in spontaneously hypertensive rats via interactions with nitric oxide. *Free Radic Biol Med.* 2005;38:450–462.
36. Tanaka M, Umemoto S, Kawahara S, et al. Angiotensin II type 1 receptor antagonist and angiotensin-converting enzyme inhibitor altered the activation of Cu/Zn-containing superoxide dismutase in the heart of stroke-prone spontaneously hypertensive rats. *Hypertens Res.* 2005;28: 67–77.
37. Romero RM, Canuelo A, Lara EM, et al. Aging affects but does not eliminate the enzymatic antioxidative response to hypoxia/reoxygenation in cerebral cortex. *Exp Gerontol.* 2006;41:25–31.
38. Iwanaga Y, Ueno M, Ueki M, et al. The expression of osteopontin is increased in vessels with blood-brain barrier impairment. *Neuropathol Appl Neurobiol.* 2008;34:145–154.
39. Cibickova L, Radomir H, Stanislav M, et al. The influence of simvastatin, atorvastatin and high-cholesterol diet on acetylcholinesterase activity, amyloid beta and cholesterol synthesis in rat brain. *Steroids.* 2009;74: 13–19.
40. Kishi T, Hirooka Y, Mukai Y, et al. Atorvastatin causes depressor and sympatho-inhibitory effects with upregulation of nitric oxide synthases in stroke-prone spontaneously hypertensive rats. *J Hypertens.* 2003;21: 379–386.
41. Hu L, Zhu DN, Yu Z, et al. Expression of angiotensin II type 1 (AT1) receptor in the rostral ventrolateral medulla in rats. *J Appl Physiol.* 2002; 92:2153–2161.
42. Cibickova L, Hyspler R, Ticha A, et al. Cholesterol synthesis in central nervous system of rat is affected by simvastatin as well as by atorvastatin. *Pharmazie.* 2008;63:819–822.
43. Golomb BA, Dimsdale JE, White HL, et al. Reduction in blood pressure with statins: results from the USCD Statin Study, a randomized trial. *Arch Intern Med.* 2008;168:721–727.

Para-Hisian Pacing for a Pediatric Patient with a Congenitally Corrected Transposition of the Great Arteries (SLL)

MASAO TAKEMOTO, M.D.,*,§ ATSUHIRO NAKASHIMA, M.D.,†,§
JUN MUNEUCHI, M.D.,‡,§ KEN-ICHIRO YAMAMURA, M.D.,‡,§
YUICHI SHIOKAWA, M.D.,†,§ KENJI SUNAGAWA, M.D.,* and RYUJI TOMINAGA, M.D.†
From the *Department of Cardiovascular Medicine, †Department of Cardiovascular Surgery, and ‡Department of Pediatrics, Heart Center, Kyushu University Hospital, Fukuoka, Japan

We report a pediatric patient with a congenitally corrected transposition of the great arteries (ccTGA)(SLL) in which permanent para-Hisian pacing (PPHP) could improve dyssynchrony-associated systemic ventricular (SV) dysfunction resulting from permanent morphologic left ventricular pacing for complete atrioventricular block. Since, in patients with ccTGA(SLL), an elongated His-bundle runs medially toward the upper septum to the site of the fibrous continuity between the right-sided mitral valve and pulmonary artery, the His-bundle may easily be captured by a pacing lead, unlike in normal hearts. Thus, PPHP may be an effective therapeutic strategy for the treatment of dyssynchrony-associated SV dysfunction associated with ccTGA (SLL). (PACE 2010; 33:e4–e7)

transposition of the great arteries, para-Hisian pacing, heart failure, cardiac resynchronization therapy, pediatrics, dyssynchrony

Introduction

The cardiac-resynchronization therapy (CRT) utilizing tranvenous biventricular pacing has become proven to produce clinical benefits in adult[1] and pediatric[2] patients with dyssynchrony-associated systemic ventricular (SV) dysfunction. Here, we report a case of prevention of ventricular desynchronization, so-called cardiac resynchronization, by utilizing transvenous permanent para-Hisian pacing (TPPHP) for dyssynchrony-associated SV dysfunction resulting from permanent morphologic left ventricular (mLV) pacing for complete atrioventricular (AV) block (CAVB) in a pediatric patient with a congenitally corrected transposition of the great arteries (ccTGA)(SLL).

Case Report

An 8-year-old girl was admitted to our hospital with a chief complaint of general fatigue and impaired daily life activities under appropriate medication with an angiotensin II receptor blocker, β-adrenergic receptor blocker, and diuretics. She had a history of repeated cardiac surgeries, consisting of a pulmonary artery banding for ccTGA(SLL), and coexisting anomalies involving an atrial septal defect (ASD) and ventricular septal defect (VSD) at a month after her birth (Fig. 1A), and the implantation of permanent epicardial pacing leads into the right atrium (RA), mLV, and SV, respectively, for CAVB following both an ASD and VSD closure at the age of 1 year (Figs. 1B and 2). The pulse generator was implanted in the intraperitoneum. Although the mLV and RA leads were still functional, the SV lead had already fractured (Fig. 2).

On admission, her blood pressure was 96/58 mmHg, and auscultation revealed a significant regurgitant systolic murmur. The electrocardiogram (ECG) revealed all ventricular pacing with a prolonged QRS duration following the intrinsic P wave (Fig. 1C). Chest X-rays revealed cardiomegaly with a 60% cardio-thoracic ratio. Her initial two-dimensional and Doppler echocardiography (UCG) revealed a severe dyssynchronous SV (morphologic RV) contraction with an SV dilation, reduced SV ejection fraction (SVEF = 19%), and severe left-sided AV (tricuspid, left) valvular regurgitation (Table I). The serum brain natriuretic peptide (BNP) was elevated to 263 pg/dL. Since we presumed the permanent mLV pacing might contribute to her SV dysfunction and heart failure (HF) progression, with left-sided AV valve regurgitation, preventative therapy with ventricular desynchronization was considered. We performed TPPHP for prevention of ventricular desynchronization, following an electrophysiological study, under general anesthesia. The bipolar screw-in leads were advanced via the left subclavian vein

There are no conflicts of interest that are related to the manuscript.

§ Contributed equally to this paper.

Address for reprints: Masao Takemoto, M.D., Ph.D., Department of Cardiovascular Medicine, Kyushu University Hospital, 3-1-1 Maidashi, Higashi-ku, Fukuoka 812-8582, Japan. Fax: 81-92-642-5374; e-mail: matakemo@cardiol.med.kyushu-u.ac.jp

Received February 20, 2009; revised March 31, 2009; accepted May 10, 2009.

doi: 10.1111/j.1540-8159.2009.02559.x

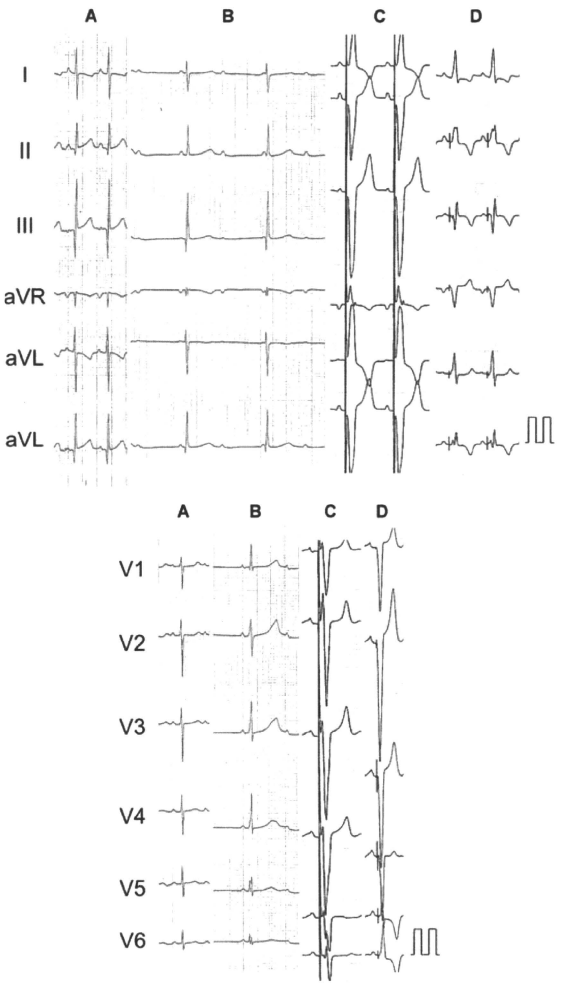

Figure 1. *The electrocardiogram during sinus rhythm at a month after her birth (A), during complete atrioventricular block at an age of 1 year (B), during epicardial morphologic left ventricular pacing on admission (QRS duration = 198 ms)(C), and during para-Hisian pacing (QRS duration = 94 ms)(D).*

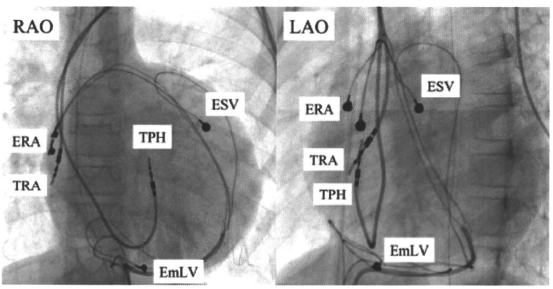

Figure 2. *Fluoroscopic images in the right (left panel) and left (right panel) anterior oblique (RAO and LAO) views. The EmLV, ERA, and ESV indicate the epicardial lead(s) in the morphologic left ventricle, right atrium, and systemic ventricle, respectively. The TPH and TRA indicate the transvenous para-Hisian pacing and transvenous right atrial leads, respectively.*

and easily positioned, using a steerable stylet into the para-His-bundle in the interventricular septum (Medtronic 5076-58, Medtronic Japan Co., Ltd, Tokyo, Japan) and RA (Medtronic 5076-52), respectively (Fig. 2), with the pulse generator (Guidant INSIGNIA I Plus DR, Guidant Japan KK, Tokyo, Japan) placed in the upper area anterior to the pectoralis major muscle of the left chest, as previously described.[3] Further, the pulse generator implanted in the intraperitoneum was turned off thereafter. The pacing threshold of the para-His-bundle lead was 0.7 Volt. The AV delay was optimized at 120 ms by UCG. TPPHP exhibited a concordant QRS axis with a native QRS (Fig. 1A and D), and could dramatically shorten the QRS duration of the ECG (Fig. 1C and D) and decrease the degree of left-sided AV valvular regurgitation as determined by UCG in accordance with an improvement in the dyssynchronous SV contraction (Table I). These conditions met the requirements of a successful criteria for TPPHP as previously defined.[4] Finally, her daily life activities steadily improved thereafter. Six months after the procedures, her clinical status, cardiomegaly, SVEF, dyssynchronous SV contraction, and serum BNP level all improved (Table I).

Discussion

Recent clinical trials have revealed that permanent right ventricular pacing could promote a dyssynchronous ventricular contraction leading to SV dysfunction and HF progression in adult patients,[5] and also contribute to adverse histological remodeling and eventual contractile dysfunction in pediatric patients.[6] A previous clinical study demonstrated that TPPHP may be one therapeutic strategy for the prevention of ventricular desynchronization in adult patients.[4]

In patients with ccTGA(SLL), the AV node is located well outside Koch's triangle, typically in an anterior and slightly lateral location within the RA, and an elongated His-bundle runs

Table I.

Parameters before and after Para-Hisian Pacing

	Before	After
Echocardiographical evaluation		
Systemic ventricular ejection fraction (%)	19	25
End-diastolic diameter of the systemic ventricle (mm)	64	63
Left-sided atrioventricular valve regurgitation (degree)	4	1
Interventricular delay[8] (milliseconds)	137	37
Other parameters		
QRS duration of the electrocardiogram (milliseconds)	198	94
New York Heart Association functional class	III	II
Serum brain natriuretic peptide (pg/dl)	263	151
Cardio-thoracic ratio (%)	60	53

Before, before para-Hiscian pacing; After, 6-months after para-Hiscian pacing
The interventricular delay was calculated by echocardiography, as previously described.[8]

medially toward the upper septum to the site of the fibrous continuity between the right-sided mitral valve and pulmonary artery in that region.[7] Thus, the His-bundle may easily be captured by a pacing lead unlike that in normal hearts. At present, the main limiting factor of the transvenous implantation of pacing leads in children may be the existence of the possible risk of a pacing lead distension and/or dislodgment associated with the patients' growth. It was suggested that such risk would be low, since these patients may have a slightly shorter stature; however, TPPHP may be prone to scarring and there are no long-term data on these leads, especially in children.

Thus, we performed TPPHP for prevention of ventricular desynchronization in this present case. It dramatically improved the dyssynchronous SV contraction and clinical status (Table I). In view of these findings, TPPHP may be one of the effective therapeutic strategies for the treatment of dyssynchrony-associated SV dysfunction and HF progression with ccTGA(SLL). Supporting data from large clinical trials, however, are needed before such conclusions can be made.

Acknowledgements: We thank John Martin for his linguistic assistance with this paper.

References

1. Abraham WT, Fisher WG, Smith AL, Delurgio DB, Leon AR, Loh E, Kocovic DZ, et al. Cardiac resynchronization in chronic heart failure. N Engl J Med 2002; 346:1845–1853.
2. Dubin AM, Janousek J, Rhee E, Strieper MJ, Cecchin F, Law IH, Shannon KM, et al. Resynchronization therapy in pediatric and congenital heart disease patients: An international multicenter study. J Am Coll Cardiol 2005; 46:2277–2283.
3. Deshmukh PM, Romanyshyn M. Direct His-bundle pacing: Present and future. Pacing Clin Electrophysiol 2004; 27:862–870.
4. Occhetta E, Bortnik M, Magnani A, Francalacci G, Piccinino C, Plebani L, Marino P. Prevention of ventricular desynchronization by permanent para-Hisian pacing after atrioventricular node ablation in chronic atrial fibrillation: A crossover, blinded, randomized study versus apical right ventricular pacing. J Am Coll Cardiol 2006; 47:1938–1945.
5. Sweeney MO, Hellkamp AS, Ellenbogen KA, Greenspon AJ, Freedman RA, Lee KL, Lamas GA. Adverse effect of ventricular pacing on heart failure and atrial fibrillation among patients with normal baseline QRS duration in a clinical trial of pacemaker therapy for sinus node dysfunction. Circulation 2003; 107:2932–2937.
6. Karpawich PP. Chronic right ventricular pacing and cardiac performance: The pediatric perspective. Pacing Clin Electrophysiol 2004; 27:844–849.
7. Anderson RH, Arnold R, Wilkinson JL. The conducting system in congenitally corrected transposition. Lancet 1973; 1:1286–1288.
8. Jauvert G, Rousseau-Paziaud J, Villain E, Iserin L, Hidden-Lucet F, Ladouceur M, Sidi D. Effects of cardiac resynchronization therapy on echocardiographic indices, functional capacity, and clinical outcomes of patients with a systemic right ventricle. Europace 2008.

Am J Physiol Heart Circ Physiol 298: H1966–H1975, 2010.
First published March 26, 2010; doi:10.1152/ajpheart.00340.2009.

Parallel resetting of arterial baroreflex control of renal and cardiac sympathetic nerve activities during upright tilt in rabbits

Atsunori Kamiya, Toru Kawada, Masaki Mizuno, Shuji Shimizu, and Masaru Sugimachi
Department of Cardiovascular Dynamics, National Cardiovascular Centre Research Institute, Suita, Japan

Submitted 8 April 2009; accepted in final form 23 March 2010

Kamiya A, Kawada T, Mizuno M, Shimizu S, Sugimachi M. Parallel resetting of arterial baroreflex control of renal and cardiac sympathetic nerve activities during upright tilt in rabbits. *Am J Physiol Heart Circ Physiol* 298: H1966–H1975, 2010. First published March 26, 2010; doi:10.1152/ajpheart.00340.2009.—Since humans are under ceaseless orthostatic stress, the mechanisms to maintain arterial pressure (AP) against gravitational fluid shift are important. As one mechanism, it was reported that upright tilt reset baroreflex control of renal sympathetic nerve activity (SNA) to a higher SNA in anesthetized rabbits. In the present study, we tested the hypothesis that upright tilt causes a parallel resetting of baroreflex control of renal and cardiac SNAs in anesthetized rabbits. In anesthetized rabbits (n = 8, vagotomized and aortic denervated) with 0° supine and 60° upright tilt postures, renal and cardiac SNAs were simultaneously recorded while isolated intracarotid sinus pressure (CSP) was increased stepwise from 40 to 160 mmHg with increments of 20 mmHg. Upright tilt shifted the reverse-sigmoidal curve of the CSP-SNA relationship to higher SNA similarly in renal and cardiac SNAs. Although upright tilt increased the maximal gain, the response range and the minimum value of SNA, the curves were almost superimposable in these SNAs regardless of postures. Scatter plotting of cardiac SNA over renal SNA during the stepwise changes in CSP was close to the line of identity in 0° supine and 60° upright tilt postures. In addition, upright tilt also shifted the reverse-sigmoidal curve of the CSP-heart rate relationship to a higher heart rate, with increases in the maximal gain and the response range. In conclusion, upright posture caused a resetting of arterial baroreflex control of SNA similarly in renal and cardiac SNAs in anesthetized rabbits.

blood pressure; orthostasis; sympathetic nervous system

SINCE HUMANS ARE UNDER CEASELESS orthostatic stress, the mechanisms to maintain arterial pressure (AP) against gravitational fluid shift are greatly important. During standing, a gravitational fluid shift directed toward the lower part of the body (such as the abdominal vascular bed and lower limbs) will cause severe postural hypotension if not counteracted by compensatory mechanisms (15). Arterial baroreflexes have been considered to be the major compensatory mechanism (1, 13, 15), since denervation of baroreceptor afferents causes profound postural hypotension (16). In addition, we (8) recently reported that upright tilt resets baroreflex control of sympathetic nerve activity (SNA) to higher SNA. The resetting doubles SNA, compensates for the reduced pressor responses of cardiovascular organs to SNA during gravitational stress, and contributes to prevent postural hypotension. However, since the study recorded only renal SNA, it remains unknown whether upright tilt resets arterial baroreflex control of SNA innervating cardiovascular organs (i.e., the heart) other than the kidney. Since cardiac SNA has a critical role in circulation, baroreflex control of cardiac SNA during orthostatic stress is of importance.

Accordingly, in the present study, we tested the hypothesis that upright tilt causes a parallel resetting of arterial baroreflex control of renal and cardiac SNAs in anesthetized rabbits. Since total baroreflex is a closed-loop negative feedback system that senses baroreceptor pressure and controls AP, and since the baroreflex control of SNA (from baroreceptor pressure input to SNA) is a subsystem of the total baroreflex system, it is difficult to isolate the baroreflex control of SNA from the total system in the baroreflex closed-loop condition (16). Therefore, we opened the baroreflex feedback loop by vascularly isolating the carotid sinus region and loaded artificial stepwise intracarotid sinus pressure (CSP) in anesthetized rabbits. By recording renal and cardiac SNAs simultaneously, we investigated static characteristics of baroreflex control of these SNAs (CSP-SNA relationship) in 0° and 60° upright tilt postures.

METHODS

Animals, preparation, and measurements. Japanese White rabbits weighing 2.4–3.3 kg were used. Animals were cared for in strict accordance with the "Guiding Principles for the Care and Use of Animals in the Field of Physiological Science" approved by the Physiological Society of Japan.

Animals (n = 8) were initially anesthetized by intravenous injection (2 ml/kg) of a mixture of urethane (250 mg/ml) and α-chloralose (40 mg/ml). Anesthesia was maintained by continuously infusing the anesthetics at a rate of 0.33 $ml \cdot kg^{-1} \cdot h^{-1}$ using a syringe pump (CFV-3200; Nihon Kohden, Tokyo, Japan). The rabbits were mechanically ventilated with oxygen-enriched room air. Bilateral carotid sinuses were isolated vascularly from the systemic circulation by ligating the internal and external carotid arteries and other small branches originating from the carotid sinus regions. The isolated carotid sinuses were filled with warmed physiological saline, pre-equilibrated with atmospheric air, through catheters inserted via the common carotid arteries. The intracarotid sinus pressure (CSP) was controlled by a servo-controlled piston pump (model ET-126A; Labworks, Costa Mesa, CA). Bilateral vagal and aortic depressor nerves were sectioned in the middle of the neck region to eliminate reflexes from the cardiopulmonary region and the aortic arch. The systemic AP was measured using a high-fidelity pressure transducer (Millar Instruments, Houston, TX) inserted retrograde from the right common carotid artery below the isolated carotid sinus region. Heart rate (HR) was measured with a cardiotachometer (model N4778; San-ei, Tokyo, Japan).

Body temperature was maintained at around 38°C with a heating pad. The left renal sympathetic nerve was exposed retroperitoneally, and the left cardiac sympathetic nerve was exposed through a middle thoracotomy. A pair of stainless steel wire electrodes (Bioflex wire AS633; Cooner Wire) was hooked onto each of these nerves to record renal and cardiac SNAs. The nerve fibers peripheral to electrodes were ligated securely and crushed to eliminate afferent signals. The nerve

Address for reprint requests and other correspondence: A. Kamiya, Dept. of Cardiovascular Dynamics, National Cardiovascular Centre Research Institute, Suita 565-8565, Japan (e-mail: kamiya@ri.ncvc.go.jp).

and electrodes were covered with a mixture of silicone gel (silicon low viscosity, Kwik-Sil; World Precision Instruments, Sarasota, FL) to insulate and immobilize the electrodes. The preamplified SNA signals were band-pass filtered at 150–1,000 Hz. These nerve signals were full-wave rectified and low-pass filtered with a cutoff frequency of 30 Hz to quantify the nerve activity. After the experiment, an intravenous infusion of hexamethonium bromide (6 mg/kg) abolished the SNA signals, indicating that the signals recorded were postganglionic SNA.

Protocols. After the preparation, the animal was maintained in a 0° supine posture on a tilt bed. To stabilize the posture, the head was fixed full-frontal to the bed by strings, and the body and legs were rigged up in a clothes-like bag. Bilateral CSP was artificially controlled independently of systemic AP. First, actual operating pressure and SNAs under baroreflex closed-loop conditions in the 0° supine posture were obtained. The animal was kept in the 0° supine posture for 10 min while CSP was matched with systemic AP via the servo-controlled piston pump.

Second, the static characteristics of the sympathetic baroreflex system were estimated in the 0° position under baroreflex open-loop conditions. The animal was kept in the 0° supine posture while CSP was decreased to 40 mmHg and then increased stepwise from 40 to 160 mmHg in increments of 20 mmHg. Each CSP step was maintained for 60 s.

Third, actual operating pressure and SNAs under baroreflex closed-loop conditions in the 60° upright tilt position were obtained. The animal was kept supine for 10 min and then tilted upright to 60° within 10 s by inclining the tilt bed to 60° and dropping the lower regions of the rabbit with the fulcrum set at the level of the carotid sinus. The 60° upright posture was maintained for 10 min. CSP was matched with systemic AP via the servo-controlled piston pump. Since the clothes-like bag stabilized the posture of the animals, there was no additional mechanical movement that reduced the quality of measurements. The position of the head remained almost fixed during the tilt to minimize vestibular stimulation. Last, the static characteristics of the sympathetic baroreflex system were estimated during the 60° upright tilt posture. CSP was increased stepwise from 40 to 160 mmHg similarly to the experiment in the 0° position. These SNAs and AP were recorded at a 200-Hz sampling rate using a 12-bit analog-to-digital converter and stored on the hard disk of a dedicated laboratory computer system for later analysis.

Data analysis. The SNA signals were normalized by the following steps. First, for each type of SNA, 0 arbitrary unit (a.u.) was assigned to the postmortem noise level. Second, 100 a.u. were assigned to the average of actual operating SNA values during baseline period in 0° positions. Last, the other SNA signals were then normalized to these values in each experiment.

These SNA and HR values were averaged for the last 10 s of each CSP level. The static relationships between CSP and SNA and between CSP and HR were parameterized by two widely used traditional models (nonlinear reverse-sigmoidal curve, linear regression line), although both models have limited abilities to reproduce the actual data. In the former case, the data were parameterized by a four-parameter logistic equation model as follows:

$$Y = P_4 + \frac{P_1}{1 + \exp[P_2(CSP - P_3)]} \quad (1)$$

where Y is SNA or HR, P_1 is the response range of Y (i.e., the difference between the maximum and minimum values of Y), P_2 is the coefficient of gain, P_3 is the midpoint CSP of the logistic function, and P_4 is the minimum value of Y. We calculated the instantaneous gain

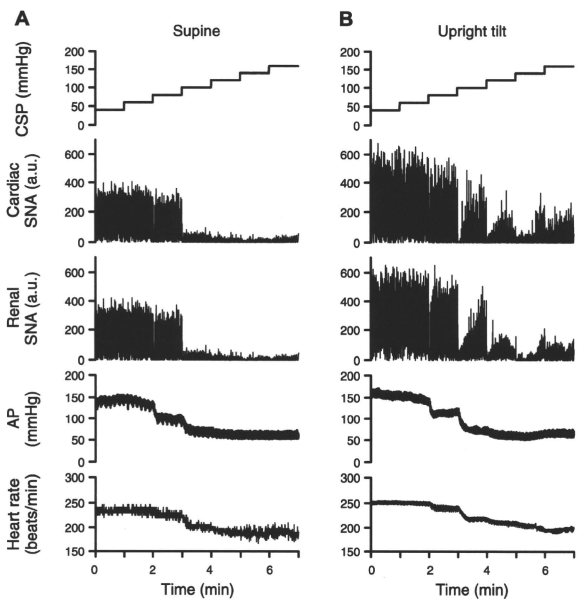

Fig. 1. Representative time series of renal and cardiac sympathetic nerve activities (SNAs) and arterial pressure (AP) in response to a stepwise increase in intracarotid sinus pressure (CSP) in 0° supine (*A*) and 60° upright tilt postures (*B*) obtained from 1 animal. Each CSP step was maintained for 1 min. All data were sampled at 10 Hz. In both SNAs, increasing CSP decreased SNAs in both postures, but upright tilt increased SNAs at all CSP levels. a.u., Arbitrary unit.

from the first derivative of the logistic function and the maximum gain (G_{max}) from $-P_1P_2/4$ at CSP = P_3.

Statistic analysis. All data are means ± SD. Effects of the upright tilt on baroreflex parameters were evaluated by repeated-measures analysis of variance. When the main effect was found to be significant, post hoc multiple comparisons were made using Scheffé's *F*-test to compare baroreflex controls between renal and cardiac SNAs (3). Differences were considered significant when $P < 0.05$.

RESULTS

Baroreflex control of renal and cardiac SNAs. Figure 1 shows the representative time series data obtained from one subject. The renal and cardiac SNAs similarly decreased in response to stepwise increase in CSP in the 0° supine posture (Fig. 1*A*). The 60° upright tilt increased these SNAs at each CSP level (Fig. 1*B*) compared with the supine posture.

Figure 2 shows the relationship between CSP and SNA in the same data as in Fig. 1*A*. In Fig. 2, these SNAs were averaged for the last 10 s of each CSP level to investigate the steady-state, not transient, response to a stepwise change in CSP. The 60° upright tilt increased renal (Fig. 2*A*) and cardiac SNAs (Fig. 2*C*) at all CSP levels compared with the supine posture. The renal SNA approximately matched the cardiac SNA at all CSP levels in the supine posture (Fig. 2*B*) and also in the upright tilt posture (Fig. 2*D*).

When the static relationship between CSP and each SNA was fitted to a nonlinear reverse-sigmoidal curve (Fig. 3), the r^2 value was ~0.95. The 60° upright tilt shifted the CSP-renal SNA curve upward to a higher SNA (Fig. 3*A*). Similarly, the upright tilt shifted the CSP-cardiac SNA curve (Fig. 3*C*) in the same manner as renal SNA. The CSP-renal SNA curve was almost superimposed on the CSP-cardiac SNA curve in the 0° supine (Fig. 3*B*) and upright tilt postures (Fig. 3*D*). However, the model was limited in reproducing the data, since the measured SNAs did not saturate at the CSP levels of 40–60 mmHg.

When the static relationship between CSP and each SNA was fitted to a linear regression line (Fig. 4), the r^2 value was 0.82–88, lower than when the nonlinear reverse-sigmoidal curve was used. The 60° upright tilt shifted the CSP-renal SNA (Fig. 4*A*) and the CSP-cardiac SNA lines (Fig. 4*C*) upward to the higher SNA levels. The CSP-renal SNA line was almost superimposed on the CSP-cardiac SNA line in the 0° supine (Fig. 4*B*) and upright tilt postures (Fig. 4*D*).

Averaged data from all animals showed that the 60° upright tilt increased renal (Fig. 5*A*) and cardiac SNAs (Fig. 5*B*) at all CSP levels compared with the 0° supine posture. The renal SNA almost matched the cardiac SNA at all CSP levels in the supine (Fig. 5*D*) and also in the upright tilt posture (Fig. 5*E*),

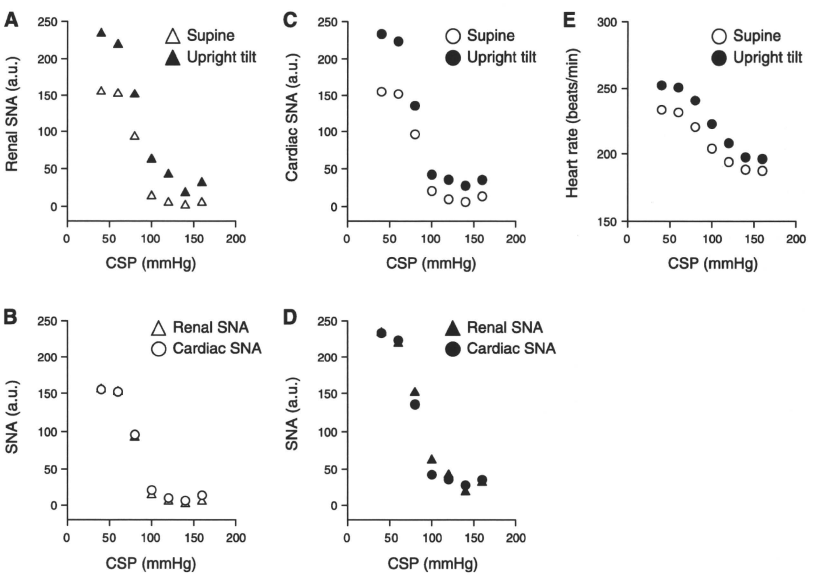

Fig. 2. Example of arterial baroreflex control of renal (*A*) and cardiac SNAs (*C*) and heart rate (HR; *E*). Data were obtained from the same animal studied in Fig. 1 and averaged for the last 10 s of each CSP level. Open and filled symbols show the data in the supine and 60° upright tilt postures, respectively. The upright tilt shifted the baroreflex control of SNA to a higher SNA similarly in the CSP-renal SNA (*A*) and CSP-cardiac SNA relationships (*C*). Data in *B* and *D* represent the superimposing of baroreflex control of SNA between renal and cardiac SNAs in both the supine and upright tilt postures, respectively. The upright tilt also shifted the baroreflex control of HR upward (*E*).

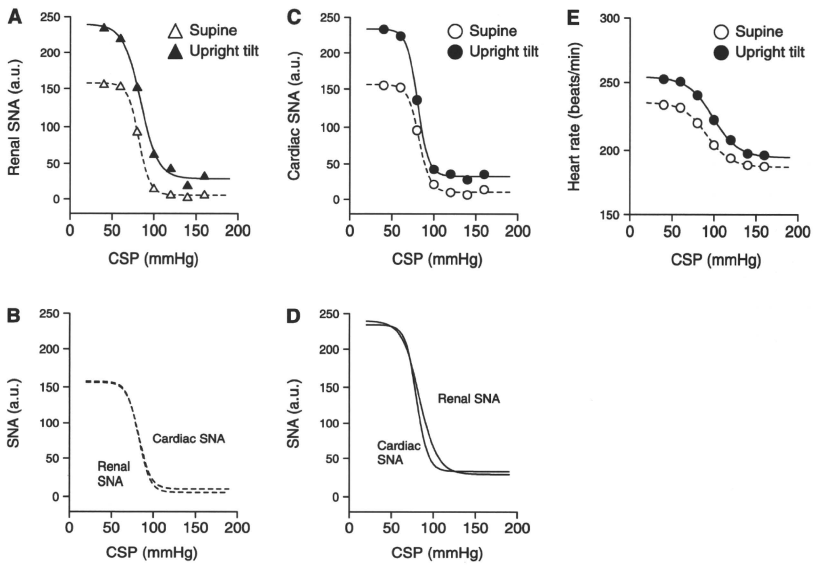

Fig. 3. Example of a model of the data shown in Fig. 2 using reverse-sigmoid 4-parameter logistic functions. Dotted and solid curves show the data in the supine and 60° upright tilt postures, respectively. The upright tilt shifted the baroreflex curves to a higher SNA similarly in renal (*A*) and cardiac SNAs (*C*). The curves were superimposed between these SNAs in the supine (*B*) and upright tilt postures (*D*). The upright tilt also shifted the baroreflex curve of HR upward (*E*).

indicating that 60° upright tilt shifted the CSP-SNA relationship upward by similar magnitudes in renal and cardiac SNAs.

When the static relationship between CSP and each SNA was fitted to a nonlinear reverse-sigmoidal curve (Fig. 6), the upright tilt shifted the CSP-SNA curve to higher SNA similarly in renal (Fig. 6*A*) and cardiac SNAs (Fig. 6*C*). The CSP-SNA relationship was almost superimposed between these SNAs in both the supine (Fig. 6*B*) and upright tilt postures (Fig. 4*D*). In both renal and cardiac SNAs, P_1 (the range of SNA response to CSP), P_4 (the minimum value of SNA), and the maximal gain (at the midpoint of the logistic function) were larger at upright tilt than supine posture (Table 1), whereas P_2 (the coefficient of gain) and P_3 (the midpoint CSP of the logistic function) were not different between postures (Table 1). In both postures, these parameters of P_{1-4} and maximal gain were similar in renal and cardiac SNAs (Table 1).

When the static relationship between CSP and each SNA was fitted to a linear regression line (Fig. 7), the upright tilt shifted the CSP-SNA line to higher SNA similarly in renal (Fig. 7*A*) and cardiac SNAs (Fig. 7*C*). It increased the slope of regression from -1.4 ± 0.3 to -1.8 ± 0.3 a.u./mmHg in renal SNA and from -1.4 ± 0.3 to -1.8 ± 0.4 a.u./mmHg in cardiac SNA. The CSP-SNA lines were almost superimposed on their SNAs in the 0° supine (Fig. 7*B*) and also the upright tilt posture (Fig. 7*D*). In both SNAs of all animals, the r^2 value was always lower (0.80–0.89) than when a nonlinear reverse-sigmoidal curve was used (0.92–0.97).

In addition, in both 0° supine and 60° upright tilt postures, scatter plotting of cardiac SNA over renal SNA was approximately close to the line of identity for each subject (Fig. 8A) and the pooled data from all subjects (Fig. 8*B*), indicating that these SNAs changed in parallel in response to stepwise increase in CSP regardless of posture. The upright tilt did not change operating AP (steady-state AP: 102 ± 4 mmHg in supine posture, 102 ± 5 mmHg in upright tilt posture). The upright tilt increased operating renal (100 a.u in supine posture, 148 ± 19 a.u. in upright posture) and cardiac SNAs (100 a.u in supine posture, 155 ± 21 a.u. in upright posture) by similar magnitudes.

Figure 9 showed the discharge characteristics of the renal and cardiac SNAs obtained from the same animal studied in Fig. 1. These SNAs were similar to some extent regardless of baroreflex condition and posture. In the supine posture (Fig. 9*A*), first, these SNAs were weakly pulse synchronous and had slower fluctuations with a time cycle of ~1.7 s in the baroreflex closed-loop condition, where CSP was artificially matched with systemic AP. The CSP and AP also had fluctuations with the same time cycle. Second, in the baroreflex open-loop condition, where CSP was fixed at 40 mmHg (the CSP level was chosen because it maximized these SNAs) without pulse, these SNAs had neither a pulse rhythmicity nor the slower fluctuation observed in the closed-loop condition. These discharge characteristics of SNAs were also observed in the 60° upright posture (Fig. 9*B*), although the amplitude of SNAs were larger at upright tilt than supine posture.

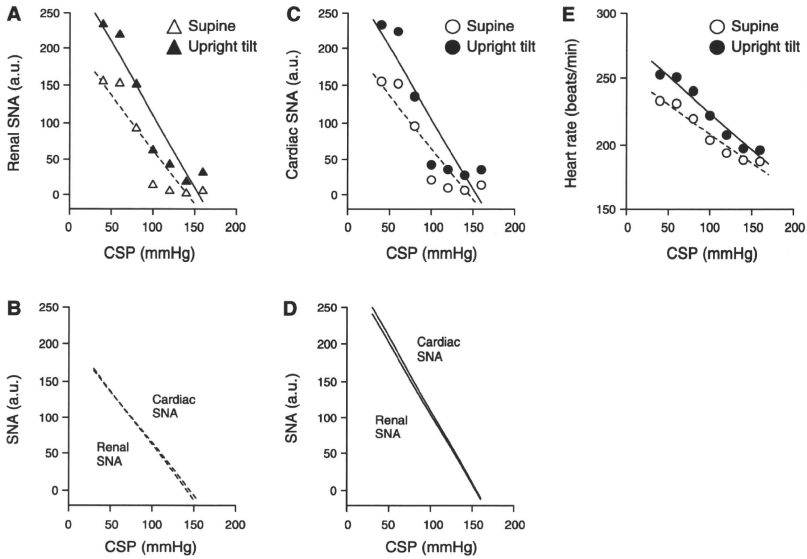

Fig. 4. Example of a model of the data shown in Fig. 2 using a simple regression line. Dotted and solid lines show the data in the supine and 60° upright tilt postures, respectively. The upright tilt shifted the baroreflex lines to a higher SNA similarly in renal (*A*) and cardiac SNAs (*C*). The lines were superimposed between these SNAs in the supine (*B*) and upright tilt postures (*D*). The upright tilt also shifted the baroreflex line of HR upward (*E*).

Baroreflex control of HR. In the representative time-series data, HR decreased in response to a stepwise increase in CSP in the 0° supine posture (Fig. 1*A*) and during 60° upright tilt (Fig. 1*B*). The upright tilt shifted the CSP-HR relationship upward to a higher HR (Fig. 2*E*), although HR was averaged for the last 10 s of each CSP level to investigate the steady-state, not transient, response to stepwise change in CSP.

Averaged data from all animals showed that the upright tilt shifted the CSP-HR relationship upward to a higher HR (Fig. 5*E*). When the static relationship between CSP and HR was fitted to a nonlinear reverse-sigmoidal curve (Fig. 6*E*), the P_1 (the range of HR response to CSP) and the maximal gain (at the midpoint of the logistic function) were larger at upright tilt than in the supine posture (Table 2), whereas P_2 (the coefficient of gain), P_3 (the midpoint CSP of the logistic function), and P_4 (the minimum value of HR) were not different between postures (Table 2). When the static relationship between CSP and HR was fitted to a linear regression line (Fig. 8*E*), the upright tilt increased the slope of regression from 0.46 ± 0.3 to 0.60 ± 0.3 beats·min^{-1}·mmHg^{-1}. The upright tilt increased operating HR (steady-state HR; 204 ± 11 beats/min in supine posture, 220 ± 12 beats/min in upright tilt posture).

DISCUSSION

Arterial baroreflex control of SNA is considered to have an important role to maintain AP under orthostatic stress against gravitational fluid shift directed toward the lower part of the body (15). In addition, we (8) recently reported that upright tilt resets arterial baroreflex control of renal SNA to increase orthostatic sympathetic activation. However, it remains unknown whether upright tilt resets arterial baroreflex control of SNA innervating to cardiovascular organs (i.e., the heart) other than the kidney. One major new finding in this study is that 60° upright tilt resets arterial baroreflex control of SNA to higher SNA similarly in renal and cardiac SNAs. This supports our hypothesis that upright tilt causes a parallel resetting of arterial baroreflex control of renal and cardiac SNAs in anesthetized rabbits.

Some regional differences between renal and cardiac SNAs certainly have been reported under some physiological conditions. First, for example, the dynamic high-pass characteristics in baroreflex control of SNA were greater in cardiac SNA than renal SNA (6, 10). Second, activating left atrial receptors increased cardiac SNA but decreased renal SNA (9). Last, hypoxia reset the AP-SNA relationship to higher AP and SNA in renal SNA but to lower AP and SNA in cardiac SNA (4). These lines of evidence indicate that renal and cardiac SNAs respond differently to specific physiological stimulation and stress (14).

However, our results indicate that upright posture induces a parallel resetting in arterial baroreflex control of renal and cardiac SNAs in the static characteristics. In agreement with previous studies (6, 7), the CSP-renal SNA reverse-sigmoidal curve was superimposable to the CSP-cardiac SNA curve in

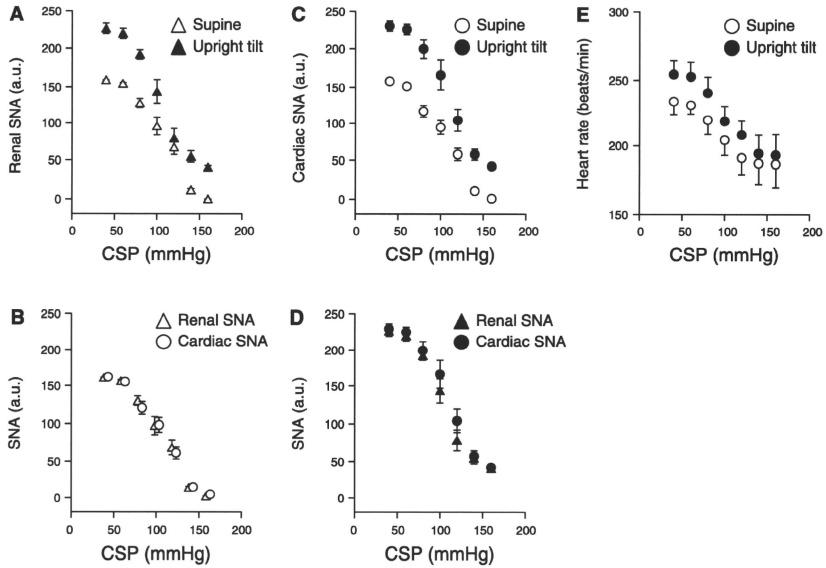

Fig. 5. Averaged data of arterial baroreflex control of renal (*A*) and cardiac SNAs (*C*) and HR (*E*) from all animals (n = 8). Open and filled symbols show the data in the supine and 60° upright tilt postures, respectively. The upright tilt shifted the baroreflex control of SNA to a higher SNA similarly in the CSP-renal SNA (*A*) and CSP-cardiac SNA relationships (*C*). *B* and *D* represent the superimposing of baroreflex control of SNA between renal and cardiac SNAs in both the supine and upright tilt postures, respectively. The upright tilt also shifted the baroreflex control of HR upward (*E*). Data are means ± SD.

the supine posture. This indicates that static nonlinear characteristics in arterial baroreflex control of renal SNA matched those of cardiac SNA in the posture. In addition, since upright tilt posture shifted the CSP-SNA curves upward similarly in renal and cardiac SNAs, the static nonlinear characteristics in arterial baroreflex control of renal SNA also matched those of cardiac SNA in upright tilt posture. These results were consistent with the close correlation between renal and cardiac SNAs during forced CSP changes with supine and upright tilt postures. They might also be consistent with a numerical simulation study indicating parallel responses of renal and cardiac SNAs to physiological pressure perturbations (AP change) (6).

Our results indicate that upright posture resets arterial baroreflex control of HR to a higher HR. This is consistent with the results of baroreflex resetting for cardiac SNA under upright tilt, because the P_I (the response range) and the maximal gain (at the midpoint of the logistic function) were larger in both CSP-HR and CSP-cardiac SNA relationships. The parallelism suggests that cardiac sympathetic efferent was a dominant determinant for HR in the present experimental condition with cutting of vagal nerves. Our results could be consistent with the increase in the baroreflex gain for HR assessed by a neck pressure/suction device in humans (11).

Limitations. The present study has several limitations. First, we excluded the efferent effect of vagally mediated arterial baroreflex and an anesthetic agent that could affect baroreflex control of SNA. Second, the vascular isolation of carotid sinus might decrease brain blood flow under, in particular, upright tilt position. Third, we eliminated cardiopulmonary baroreflex by cutting bilateral vagal nerves. Earlier human studies have indicated that nonhypotensive hypovolemic perturbations do not change AP but reduce central venous, right heart, and pulmonary pressures and cause vasoconstriction. These observations have been interpreted as reflexes triggered by cardiopulmonary baroreceptors (5, 12). However, Taylor et al. (17) showed that small reductions of effective blood volume reduce aortic baroreceptive areas and trigger hemodynamic adjustments that are so efficient that alterations in AP escape detection by conventional means. In addition, Fu et al. (2) reported that arterial baroreceptors are consistently unloaded during low levels (i.e., −10 and −15 mmHg) of lower body negative pressure in humans. Accordingly, further studies are needed to understand the relative importance and mutual cooperation of arterial and cardiopulmonary baroreflexes in AP control during orthostatic stress. Fourth, we investigated arterial baroreflex during upright posture in rabbits, which are quadripeds. However, denervation of both carotid and aortic arterial baroreflexes caused postural hypotension of ~50 mmHg during 60° upright tilt in quadripeds [rabbits and rats (16)]. This suggests that even in quadripeds, arterial baroreflex has a very important role in maintenance of AP under orthostatic stress.

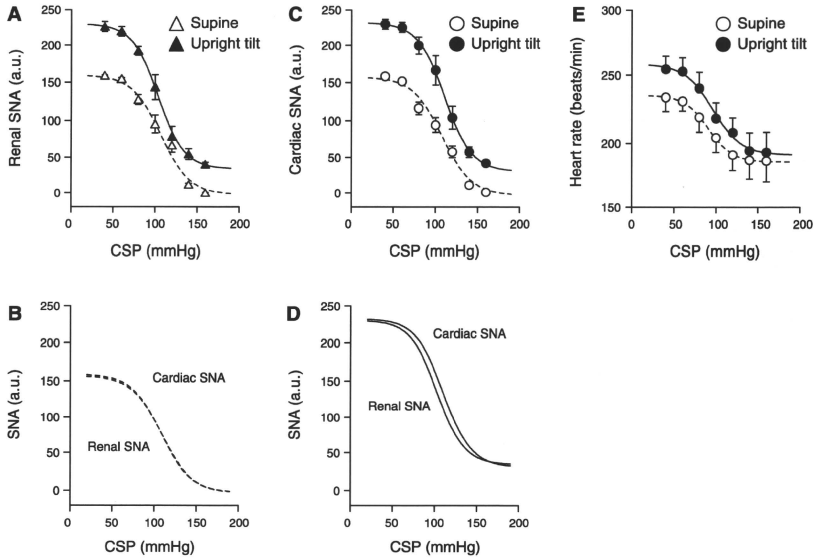

Fig. 6. A model of the averaged data shown in Fig. 5 using reverse-sigmoid 4-parameter logistic functions. Dotted and solid curves show the data in the supine and 60° upright tilt postures, respectively. The upright tilt shifted the baroreflex curves to a higher SNA similarly in renal (*A*) and cardiac SNAs (*C*). The curves were superimposed between these SNAs in the supine (*B*) and upright tilt postures (*D*). The upright tilt also shifted the baroreflex curve of HR upward (*E*).

Last, although we used two widely used traditional models to analyze the relationship between CSP and SNA, both have limited abilities to reproduce actual data. The nonlinear reverse-sigmoidal curve parameterized by a four-parameter logistic equation model provided high r^2 values (0.92–0.97) regardless of SNA type and posture. However, we failed to observe a saturation of SNA at the lowest CSP level in some cases (40 mmHg; Fig. 3, *A* and *B*, in upright tilt position). Lots of earlier studies have applied the model to AP and SNA (or HR) data under pharmacological perturbation (i.e., nitroprusside, phenylephrine) (1, 14), although it is difficult to observe clear saturation and/or threshold in the data. In contrary, the simple linear regression line model provided lower r^2 values (0.80–0.89). The plotted data did not appear to lie on a simple line in individuals (Fig. 4). Accordingly, we cannot conclude whether the relation between CSP and SNA is sigmoid or not. This problem is not the purpose of this study. Importantly, without modeling, our data (Fig. 2 and 5) indicate the parallel resetting of arterial baroreflex control of renal and cardiac SNAs.

Table 1. *Effect of upright tilt on parameters of baroreflex control of renal and catdiac SNAs*

	Supine	Upright tilt
Renal SNA		
P_1, a.u.	161 ± 2	196 ± 5*
P_2, a.u./mmHg	0.08 ± 0.01	0.08 ± 0.02
P_3, mmHg	105 ± 6	104 ± 6
P_4, a.u.	2 ± 1	34 ± 6*
G_{max}, a.u./mmHg	−1.5 ± 0.4	−1.9 ± 0.4*
Cardiac SNA		
P_1, a.u.	160 ± 2	201 ± 5*
P_2, a.u./mmHg	0.08 ± 0.01	0.08 ± 0.02
P_3, mmHg	109 ± 6	111 ± 6
P_4, a.u.	2 ± 1	31 ± 6*
G_{max}, a.u./mmHg	−1.4 ± 0.4	−1.9 ± 0.4*

Values are means ± SD (n = 8) for the parameters of baroreflex control of renal and cardiac sympathetic nerve activities (SNAs). See *Eq. 1* in METHODS for definitions of the 4 parameters of the logistic function. *$P < 0.05$, supine vs. upright tilt.

In conclusion, upright posture causes a resetting in arterial baroreflex control of SNA in parallel in renal and cardiac SNAs in anesthetized rabbits.

GRANTS

This study was supported by a research project promoted by the Ministry of Health, Labour and Welfare in Japan (no. H18-nano-ippan-003, H21-nano-ippan-005), a Grant-in-Aid for Scientific Research promoted by the Ministry of Education, Culture, Sports, Science and Technology in Japan (no. 20390462), and the Industrial Technology Research Grant Program from the New Energy and Industrial Technology Development Organization (NEDO) of Japan.

DISCLOSURES

No conflicts of interest, financial or otherwise, are declared by the author(s).

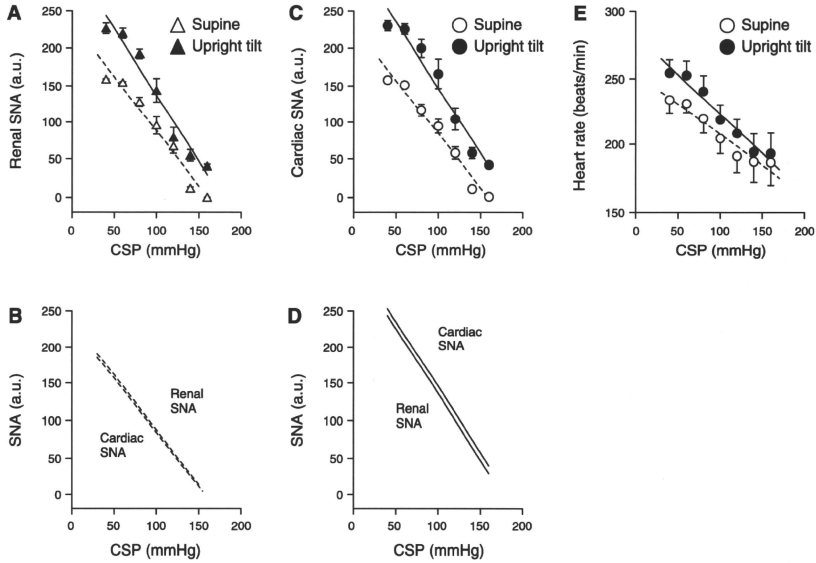

Fig. 7. A model of the averaged data shown in Fig. 5 using a simple regression line. Dotted and solid lines show the data in the supine and 60° upright tilt postures, respectively. The upright tilt shifted the baroreflex lines to a higher SNA similarly in renal (*A*) and cardiac SNAs (*C*). The lines were superimposed between these SNAs in the supine (*B*) and upright tilt postures (*D*). The upright tilt also shifted the baroreflex line of HR upward (*E*).

REFERENCES

1. **Eckberg DL, Sleight P.** *Human Baroreflexes in Health and Disease.* New York: Oxford Univ. Press, 1992, p. 3–299.
2. **Fu Q, Shibata S, Hastings JL, Prasad A, Palmer MD, Levine BD.** Evidence for unloading arterial baroreceptors during low levels of lower body negative pressure in humans. *Am J Physiol Heart Circ Physiol* 296: H480–H488, 2009.
3. **Glantz SA.** *Primer of Biostatistics* (4th ed.). New York: McGraw-Hill, 1997.
4. **Iriki M, Dorward P, Korner PI.** Baroreflex "resetting" by arterial hypoxia in the renal and cardiac sympathetic nerves of the rabbit. *Pflügers Arch* 370: 1–7, 1977.
5. **Johnson JM, Rowell LB, Niederberger M, Eisman MM.** Human splanchnic and forearm vasoconstrictor responses to reductions of right atrial and aortic pressures. *Circ Res* 34: 515–524, 1974.
6. **Kamiya A, Kawada T, Yamamoto K, Michikami D, Ariumi H, Miyamoto T, Shimizu S, Uemura K, Aiba T, Sunagawa K, Sugimachi M.** Dynamic and static baroreflex control of muscle sympathetic nerve activity (SNA) parallels that of renal and cardiac SNA during physiological change in pressure. *Am J Physiol Heart Circ Physiol* 289: H2641–H2648, 2005.
7. **Kamiya A, Kawada T, Yamamoto K, Michikami D, Ariumi H, Miyamoto T, Uemura K, Sugimachi M, Sunagawa K.** Muscle sympathetic nerve activity averaged over 1 min parallels renal and cardiac sympathetic nerve activity in response to a forced baroreceptor pressure change. *Circulation* 112: 384–386, 2005.
8. **Kamiya A, Kawada T, Yamamoto K, Michikami D, Ariumi H, Uemura K, Zheng C, Shimizu S, Aiba T, Miyamoto T, Sugimachi M, Sunagawa K.** Resetting of the arterial baroreflex increases orthostatic sympathetic activation and prevents postural hypotension in rabbits. *J Physiol* 566: 237–246, 2005.
9. **Karim F, Kidd C, Malpus CM, Penna PE.** The effects of stimulation of the left atrial receptors on sympathetic efferent nerve activity. *J Physiol* 227: 243–260, 1972.
10. **Kawada T, Shishido T, Inagaki M, Tatewaki T, Zheng C, Yanagiya Y, Sugimachi M, Sunagawa K.** Differential dynamic baroreflex regulation of cardiac and renal sympathetic nerve activities. *Am J Physiol Heart Circ Physiol* 280: H1581–H1590, 2001.
11. **Ogoh S, Yoshiga CC, Secher NH, Raven PB.** Carotid-cardiac baroreflex function does not influence blood pressure regulation during head-up tilt in humans. *J Physiol Sci* 56: 227–233, 2006.
12. **Pawelczyk JA, Raven PB.** Reductions in central venous pressure improve carotid baroreflex responses in conscious men. *Am J Physiol Heart Circ Physiol* 257: H1389–H1395, 1989.
13. **Persson P, Kirchheim H.** *Baroreceptor Reflexes: Integrative Functions and Clinical Aspects.* Berlin: Springer, 1991.
14. **Ramchandra R, Hood SG, Denton DA, Woods RL, McKinley MJ, McAllen RM, May CN.** Basis for the preferential activation of cardiac sympathetic nerve activity in heart failure. *Proc Natl Acad Sci USA* 106: 924–928, 2009.
15. **Rowell LB.** *Human Cardiovascular Control.* New York: Oxford Univ. Press, 1993, p. 3–254.
16. **Sato T, Kawada T, Sugimachi M, Sunagawa K.** Bionic technology revitalizes native baroreflex function in rats with baroreflex failure. *Circulation* 106: 730–734, 2002.
17. **Taylor JA, Halliwill JR, Brown TE, Hayano J, Eckberg DL.** "Non-hypotensive" hypovolaemia reduces ascending aortic dimensions in humans. *J Physiol* 483: 289–298, 1995.

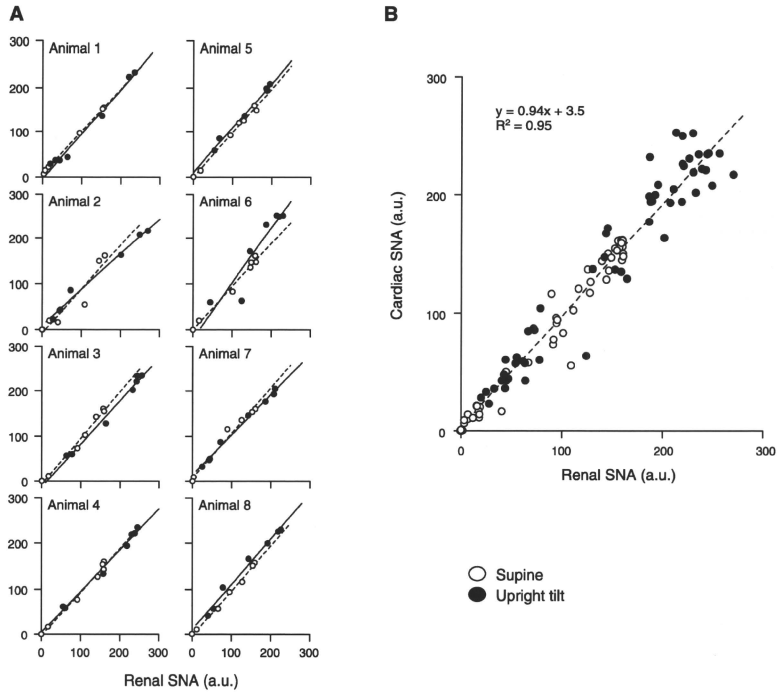

Fig. 8. Scatter plots and regression lines drawn between renal and cardiac SNAs in supine (dotted lines) and upright tilt postures (solid lines) during stepwise changes in CSP for each subject (*A*) and the pooled data from all 8 subjects (*B*).

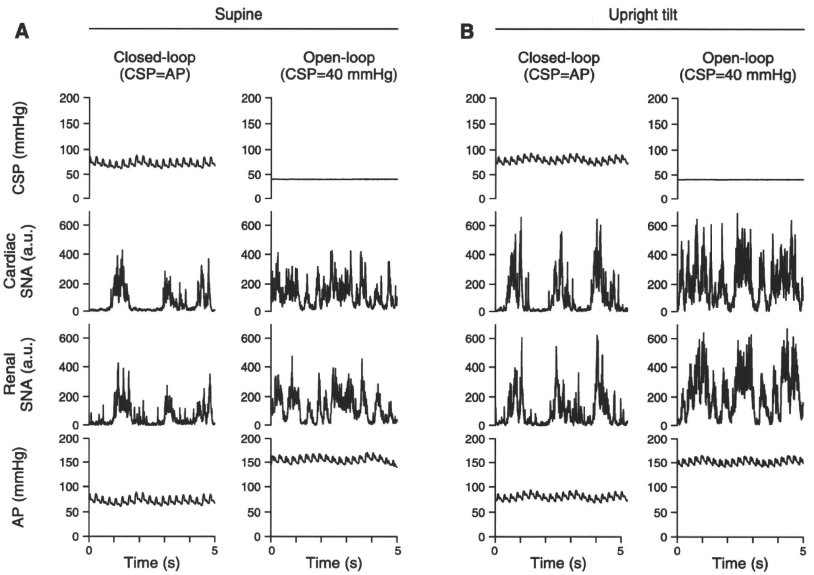

Fig. 9. Discharge characteristics of the renal and cardiac SNAs in supine (*A*) and 60° upright tilt postures (*B*) under the baroreflex closed-loop condition, where CSP was artificially matched with systemic AP, and under the open-loop condition, where CSP was fixed at 40 mmHg. Variables were resampled at 200 Hz. Data were obtained from the same animal studied in Fig. 1.

Table 2. *Effect of upright tilt on parameters of baroreflex control of HR*

	Supine	Upright tilt
P_1, beats/min	53 ± 11	67 ± 11*
P_2, beats·min^{-1}·mmHg^{-1}	0.07 ± 0.03	0.07 ± 0.03
P_3, mmHg	93 ± 8	97 ± 12
P_4, beats/min	184 ± 17	191 ± 18
G_{max}, beats·min^{-1}·mmHg^{-1}	−0.9 ± 0.2	−1.2 ± 0.4*

Values are means ± SD (n = 8) for the parameters of baroreflex control of heart rate (HR). *P < 0.05, supine vs. upright tilt.

J Physiol Sci (2010) 60:283–298
DOI 10.1007/s12576-010-0096-9

ORIGINAL PAPER

Open-loop dynamic and static characteristics of the carotid sinus baroreflex in rats with chronic heart failure after myocardial infarction

Toru Kawada · Meihua Li · Atsunori Kamiya · Shuji Shimizu · Kazunori Uemura · Hiromi Yamamoto · Masaru Sugimachi

Received: 24 January 2010 / Accepted: 5 May 2010 / Published online: 1 June 2010

Abstract We estimated open-loop dynamic characteristics of the carotid sinus baroreflex in normal control rats and chronic heart failure (CHF) rats after myocardial infarction. First, the neural arc transfer function from carotid sinus pressure to splanchnic sympathetic nerve activity (SNA) and its corresponding step response were examined. Although the steady-state response was attenuated in CHF, the negative peak response and the time to peak did not change significantly, suggesting preserved neural arc dynamic characteristics. Next, the peripheral arc transfer function from SNA to arterial pressure (AP) and its corresponding step response were examined. The steady-state response and the initial slope were reduced in CHF, suggesting impaired end-organ responses. In a simulation study based on the dynamic and static characteristics, the percent recovery of AP was reduced progressively as the size of disturbance increased in CHF, suggesting that a reserve for AP buffering is lost in CHF despite relatively maintained baseline AP.

T. Kawada (✉) · M. Li · A. Kamiya · S. Shimizu · K. Uemura · M. Sugimachi
Department of Cardiovascular Dynamics, National Cerebral and Cardiovascular Center Research Institute, 5-7-1 Fujishirodai, Suita, Osaka 565-8565, Japan
e-mail: torukawa@res.ncvc.go.jp

M. Li · S. Shimizu
Japan Association for the Advancement of Medical Equipment, Tokyo 113-0033, Japan

H. Yamamoto
Division of Cardiology, Department of Internal Medicine, Kinki University School of Medicine, Osaka 589-8511, Japan

Keywords Systems analysis · Transfer function · White noise · Sympathetic nerve activity · Arterial pressure · Equilibrium diagram

Introduction

The arterial baroreflex is an important negative feedback system that stabilizes systemic arterial pressure (AP) against exogenous disturbances. The rapidness of AP regulation may be best described by the system dynamic characteristics. With respect to the sympathetic arterial baroreflex system, previous studies in rabbits [1] and rats [2] have indicated that the transfer function of the baroreflex neural arc from baroreceptor pressure input to efferent sympathetic nerve activity (SNA) exhibits "derivative" characteristics, which means that the dynamic gain of the SNA response to pressure perturbation becomes greater as the modulation frequency increases. On the other hand, the transfer function of the baroreflex peripheral arc from SNA to AP shows "low-pass" characteristics, which means that the dynamic gain of the AP response to SNA variation becomes smaller as the modulation frequency increases. In short, the neural arc provides an accelerating mechanism of the dynamic AP response in the arterial baroreflex system [1].

Although a number of studies have indicated that the baroreflex function is depressed in heart failure [3–6], dynamic characteristics of the arterial baroreflex in heart failure have not been fully described. The aim of the present study was to identify the open-loop dynamic characteristics of the carotid sinus baroreflex in a rat model of chronic heart failure (CHF) after myocardial infarction. To obtain a total picture of the AP regulation in CHF, we also estimated the open-loop static characteristics of the carotid sinus baroreflex.

Materials and methods

Animals were cared for in strict accordance with the Guiding Principles for the Care and Use of Animals in the Field of Physiological Sciences, which has been approved by the Physiological Society of Japan. All experimental protocols were reviewed and approved by the Animal Subjects Committee at the National Cerebral and Cardiovascular Center.

Myocardial infarction

Coronary artery ligation was performed under sterile conditions in 8-week-old male Sprague-Dawley rats according to a previously established procedure [7]. After inducing anesthesia by halothane inhalation, the rat was intubated and mechanically ventilated. The left chest was opened at the fourth intercostal space and the left coronary artery was ligated with a 5-0 polypropylene suture (PROLENE, Ethicon, GA, USA). An electrocardiogram was monitored for 1 h after the coronary ligation, and the heart was defibrillated as necessary by manual prodding. Thereafter air was evacuated from the thoracic cavity and the incision was closed. The rats were allowed to recover from anesthesia, and were fed ad libitum with a standard laboratory chow and given free access to water. Although we initially planned to wait until the rats showed an objective sign of advanced heart failure such as facial edema or labored breathing, the rats with such severe heart failure were too weak to survive the acute baroreflex study described in the following section. Accordingly, the rats that survived for 100–200 days (156 ± 18 days) after myocardial infarction were used without solid criteria for starting the acute baroreflex study. Instead, the rats were regarded as experiencing CHF when the central venous pressure was higher than 2.5 mmHg or the biventricular weight was greater than 2.5 g/kg body weight at the time of the acute baroreflex study.

Acute baroreflex study

Experiments were performed in normal control ($n = 12$) and CHF ($n = 7$) rats. Sham operation was not performed in the control rats. Among the control rats, eight rats were matched with the CHF rats based on body weight, but they were younger in age due to the retardation of growth in the CHF rats. The remaining four rats were age-matched with the CHF rats, but they were heavier in body weight. Because none of the parameters of the baroreflex dynamic and static characteristics differed statistically between the two subgroups of the control rats, we report pooled data obtained from the 12 control rats.

Each rat was anesthetized with an intraperitoneal injection (2 ml/kg) of a mixture of urethane (250 mg/ml) and α-chloralose (40 mg/ml), and mechanically ventilated with oxygen-enriched room air. A venous catheter was inserted into the right femoral vein, and 20-fold diluted anesthetic mixture was administered continuously (2–3 ml kg^{-1} h^{-1}). An arterial catheter was inserted into the right femoral artery to measure AP. Heart rate (HR) was obtained from AP through a cardiotachometer. Another venous catheter was inserted into the left femoral vein and advanced into the inferior vena cava to measure central venous pressure and to supply Ringer solution (6 ml kg^{-1} h^{-1}).

A postganglionic branch from the splanchnic sympathetic nerve was exposed through a left flank incision, and a pair of stainless steel wire electrodes (Bioflex wire AS633, Cooner Wire, CA, USA) was attached to record SNA. The nerve and electrodes were covered with silicone glue (Kwik-Sil, World Precision Instruments, FL, USA) for insulation and fixation. To quantify the nerve activity, the preamplified nerve signal was band-pass filtered at 150–1,000 Hz, and then full-wave rectified and low-pass filtered with a cut-off frequency of 30 Hz. Pancuronium bromide (0.4 mg kg^{-1} h^{-1}) was administered to prevent muscular activity from contaminating the SNA recording. At the end of the experiment, we confirmed the disappearance of SNA in response to an intravenous bolus injection of a ganglionic blocker, hexamethonium bromide (60 mg kg^{-1}), and recorded the noise level.

Bilateral vagal and aortic depressor nerves were sectioned at the neck to avoid reflexes from the cardiopulmonary region and aortic arch. The carotid sinus regions were isolated from the systemic circulation bilaterally according to previously reported procedures [8, 9]. Briefly, a 7-0 polypropylene suture with a fine needle (PROLENE, Ethicon, GA, USA) was passed through the tissue between the external and internal carotid arteries, and the external carotid artery was ligated close to the carotid bifurcation. The internal carotid artery was embolized using two to three steel balls (0.8 mm in diameter, Tsubaki Nakashima, Nara, Japan) injected from the common carotid artery. Under these conditions, the brain stem area was perfused by patent bilateral vertebral arteries. The isolated carotid sinuses were filled with warmed Ringer solution through catheters inserted into the common carotid arteries. Carotid sinus pressure (CSP) was controlled using a servo-controlled piston pump. Heparin sodium (100 U kg^{-1}) was given intravenously to prevent blood coagulation. Body temperature was maintained at approximately 38°C with a heating pad.

Protocols

After the above surgical procedures were completed, reflex responses in SNA, AP, and HR to CSP input were

monitored for more than 30 min. The rat was excluded from further study and analysis in the event that the reflex responses became smaller within this period. Possible causes for the deterioration in the reflex responses include surgical damage to the carotid sinus nerves and brain ischemia due to the bilateral carotid occlusion.

To estimate the dynamic input-output relationship of the carotid sinus baroreflex, CSP was perturbed for 20 min using a Gaussian white noise (GWN) signal with the mean of 120 mmHg and standard deviation of 20 mmHg. The selection of the mean pressure and amplitude of GWN does not significantly affect the estimation of the system dynamic characteristics except for a factor of proportionality (see Appendix 1 for details). The switching interval of GWN was set at 500 ms. The input power spectral density was relatively constant up to 1 Hz, which covered the upper frequency range of interest with respect to the sympathetic arterial baroreflex in rats [2].

To estimate the static input-output relationship of the carotid sinus baroreflex, CSP was decreased to 60 mmHg for 4–6 min, and then increased stepwise from 60 to 180 mmHg in increments of 20 mmHg every minute [10].

Data analysis

Data were sampled at 200 Hz using a 16-bit analog-to-digital converter and stored on a dedicated laboratory computer system. In each rat, the noise level of SNA recorded after the administration of hexamethonium bromide was treated as zero. Because the absolute voltage of SNA varied among animals depending on the recording conditions, SNA averaged during the last 10 s at CSP of 60 mmHg in the stepwise input protocol was defined as 100%. The same normalization factor was used for the analysis of the baroreflex dynamic characteristics.

Dynamic characteristics of the baroreflex neural arc, peripheral arc, total baroreflex, and HR control were estimated by an open-loop transfer function analysis as follows [11]. Data were analyzed from 90 s after the initiation of the GWN input. The input-output data pairs were resampled at 10 Hz and segmented into 50% overlapping bins of 1,024 points each. For each segment, a linear trend was removed, and a Hanning window was applied. Fast Fourier transform was performed to obtain the frequency spectra of the input and output signals. The ensemble averages of the input power spectral density [$S_{XX}(f)$], output power spectral density [$S_{YY}(f)$], and cross spectral density between the input and output signals [$S_{YX}(f)$] were calculated over 12 segments, where f denotes frequency. Finally, the transfer function [$H(f)$] from input to output was estimated as:

$$H(f) = \frac{S_{YX}(f)}{S_{XX}(f)} \tag{1}$$

The transfer function is a complex-valued function that can be expressed by the modulus and phase at each frequency. In the present study, we refer to the modulus of the transfer function as the dynamic gain. To quantify the linear dependence between the input and output signals, a magnitude squared coherence function [Coh(f)] was calculated as:

$$\mathrm{Coh}(f) = \frac{|S_{YX}(f)|^2}{S_{XX}(f)S_{YY}(f)} \tag{2}$$

The coherence function is a real-valued function ranging from zero to unity. When the output signal is perfectly explained by the linear dynamics with the input signal, the coherence value becomes unity. When the output signal is totally independent of the input signal, the coherence value becomes zero.

To facilitate understanding of the transfer function, the step response was also calculated as follows. The system impulse response was derived from the inverse Fourier transform of $H(f)$. The step response was then obtained from the time integral of the impulse response.

To quantify the open-loop static characteristics of the carotid sinus baroreflex, mean SNA, AP, and HR were obtained during the last 10 s at each CSP level of the stepwise input protocol. In each rat, data from two consecutive step cycles were averaged. The static characteristics of the baroreflex neural arc (the CSP-SNA relationship), the total baroreflex (the CSP-AP relationship), and the HR control (the CSP-HR relationship) were described by fitting four-parameter logistic functions to the input-output data as follows [10, 12]:

$$y = \frac{P_1}{1 + \exp[P_2(x - P_3)]} + P_4 \tag{3}$$

where x and y denote the input (CSP) and output (SNA, AP, or HR), respectively; P_1 is the response range of output; P_2 is the slope coefficient; P_3 is the midpoint pressure of input; and P_4 is the minimum value of output. For convenience, the maximum slope or the maximum gain of the logistic function is reported by a positive value as $P_1P_2/4$.

The static characteristics of the baroreflex peripheral arc (the SNA-AP relationship) were quantified by a linear regression analysis as follows [10, 13]:

$$\mathrm{AP} = a \times \mathrm{SNA} + b \tag{4}$$

where a and b represent the slope and intercept, respectively, of the regression line.